

Accepted Article

Title: Reducing defects density and enhancing hole extraction for efficient perovskite solar cells enabled by π -Pb²⁺ interaction

Authors: zhongmin zhou, Li-rong Wen, Yi Rao, Mingzhe Zhu, Ruitao Li, Jingbo Zhan, Linbao Zhang, Li Wang, Ming Li, and Shuping Pang

This manuscript has been accepted after peer review and appears as an Accepted Article online prior to editing, proofing, and formal publication of the final Version of Record (VoR). This work is currently citable by using the Digital Object Identifier (DOI) given below. The VoR will be published online in Early View as soon as possible and may be different to this Accepted Article as a result of editing. Readers should obtain the VoR from the journal website shown below when it is published to ensure accuracy of information. The authors are responsible for the content of this Accepted Article.

To be cited as: *Angew. Chem. Int. Ed.* 10.1002/anie.202102096

Link to VoR: <https://doi.org/10.1002/anie.202102096>

COMMUNICATION

Reducing defects density and enhancing hole extraction for efficient perovskite solar cells enabled by π -Pb²⁺ interaction

Li-rong Wen,^{[a]†} Yi Rao,^{[b]†} Mingzhe Zhu,^[a] Ruitao Li,^[a] Jingbo Zhan,^[a] Linbao Zhang,^{*[a]} Li Wang,^{*[c]} Ming Li,^[a] Shuping Pang,^[b] and Zhongmin Zhou^{*[a]}

[a] Prof. L.-r. Wen, M. Zhu, R. Li, J. Zhan, Prof. L. Zhang, Prof. M. Li, Prof. Z. Zhou
Taishan scholar advantage and characteristic discipline team of Eco-chemical process and technology
College of Chemistry and Molecular Engineering
Qingdao University of Science and Technology
Qingdao 266042, P. R. China
E-mail: : zhang_linbao@126.com; zhouzm@qust.edu.cn

[b] Y. Rao, Prof. S. Pang
Qingdao Institute of Bioenergy and Bioprocess Technology, Chinese Academy of Sciences,
Qingdao 266101, P. R. China;
Dalian National Laboratory for Clean Energy, Dalian 116023, P.R. China

[c] Prof. L. Wang
College of Materials Science and Engineering
Qingdao University of Science and Technology
Qingdao 266042, P. R. China
E-mail: : liwang718@qust.edu.cn

[†] These authors contributed equally to this work.

Abstract: Molecular doping is an of significance approach to reduce defects density of perovskite and to improve interfacial charge extraction in perovskite solar cells. Here, we show a new strategy for chemical doping of perovskite via an organic small molecule, which features a fused tricyclic core, showing strong intermolecular π -Pb²⁺ interactions with under-coordinated Pb²⁺ in perovskite. This π -Pb²⁺ interactions could reduce defects density of the perovskite and suppress the nonradiative recombination, which was also confirmed by the density functional theory calculations. In addition, this doping via π -Pb²⁺ interactions could deepen the surface potential and downshift the work function of the doped perovskite film, facilitating the hole extraction to hole transport layer. As a result, the doped device showed high efficiency of 21.41% with ignorable hysteresis. This strategy of fused tricyclic core-based doping provides a new perspective for the design of new organic materials to improve the device performance.

Due to their high light absorption coefficient, direct and tunable bandgap, long carrier diffusion length, metal halide perovskite materials have gained significant attention in the last decade.^[1] Recent extensive research into the perovskite solar cells (PSCs) has led to power conversion efficiency (PCE) from the initial 3.8% to a certificated 25.5% and thus makes them as competitive candidates for photovoltaic applications.^[2] However, the current PCE is still far below the limit value of ~ 30% according to the theoretical Shockley-Queisser limit for single-junction solar cells, thus there is still large room for improvement.^[3] Intrinsic high defects density of perovskites and mismatched energy-level alignment at the interfaces within device could lead to robust charge recombination and inefficient charge extraction, limiting

the development of PSCs.^[4] Varieties of strategies have been exploited, among them the chemical doping is an efficient approach to reducing nonradiative recombination, improving carriers transportation and/or tuning fermi level, thus resulting in excellent device performance.^[5] For example, PCBM has been generally utilized to enhance the photoelectron transport in perovskite.^[6] Wu et al. introduced PCBM through anti-solvent into FA_{0.85}MA_{0.15}Pb(I_{0.85}Br_{0.15})₃ to construct graded heterojunction to improve the photoelectron collection and reduces charge recombination loss.^[6c] Besides, Cu(thiourea)I was utilized to passivate the trap state of perovskite (MAPbI₃Cl_{3-x}) and increase the depletion width of bulk heterojunction, which could accelerate hole transport and reduce charge recombination.^[5d] Recently, Huang group doped perovskite (MAPbI₃) with F4TCNQ to change the work function of MAPbI₃ and increase the carrier (hole) concentration and thus greatly improved device performance.^[5e]

Inspired by all above-mentioned demonstrations, we synthesize a new organic small molecule 1-(4-bromophenyl)-6,7-diphenylimidazo[5,1,2-cd]indolizine (PDPII, Figure 1), with limidazo[5,1,2-cd]indolizine as core and benzene substituents as peripheral unit. The molecule features a fused tricyclic core, showing strong intermolecular π -Pb²⁺ interactions with under-coordinated Pb²⁺ and thus reducing trap densities in perovskite. In addition, the chemical doping of **1** deepens the surface potential and increases the work function of perovskite films, facilitating the hole extraction from perovskite into hole transport

COMMUNICATION

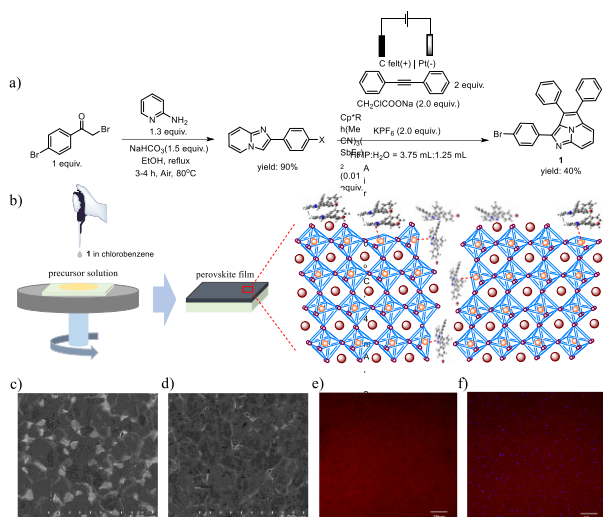


Figure 1. (a) The synthetic route to the compound **1**. (b) The schematic diagram of the deposition method of perovskite film and the compound **1** located at the grain boundary and on the surface after film formation and strongly interacted with perovskite component (Pb²⁺). SEM images of perovskite films without doping (c) and with doping (d). In situ photoluminescence maps (excitation at 405 nm and emission between 425-475 nm) of perovskite films without doping (e) and with doping (f).

layer (HTL) while reducing the charge recombination at this interface. As a result, the PCE of 21.41% was obtained with less hysteresis (21.41% and 21.34% under reverse and forward scan directions) compared with the reference device (20.22% and 18.22% under reverse and forward scan directions).

PDPII can be readily synthesized in two steps from commercial compounds. Figure 1a shows the synthetic route of **1** through the typical reaction of 2-aminopyridines and α -bromo-ketones in alkaline environment followed by hot electrochemical synthesis, which provides an environmentally-friendly approach avoiding the usage of toxic oxidants and costly additives. The compound **1** was introduced into the perovskite (FA_{0.85}MA_{0.15}Pb(I_{0.85}Br_{0.15})_{3-x}Cl_x) film via commonly utilized antisolvent dripping approach as shown in Figure 1b.^[7] Figure 1c, d exhibit the scanning electron microscopy (SEM) images of perovskite films without and with doping the compound **1**. There is no obvious difference in the grain size between the perovskite films with and without the doping, which is consistent with the cross-sectional morphology as shown in Figure S1. This doping is different from the as-reported results, which exploited varieties of dopants to modulate the crystallization of the perovskite films, showing large difference in film morphology.^[8] What's more, we don't observe new peaks appearing as demonstrated by X-ray diffraction (XRD) pattern spectra in Figure S2, indicating that there are no new phases or intermediates obtained after doping. Noting that the less intensity of pattern peaks in doped film may result from the thin layer of compound **1** on the surface of perovskite film. We can see from Figure 1d that the compound **1** is distributed at the grain

boundaries and on the surface of perovskite films, which is also confirmed by the sequence of photoluminescence (PL) maps of perovskite films taken in situ (Figure 1 e, f). We can see from Fig. 1f that the blue dots (PDPII) are uniformly distributed in the perovskite film compared to the Fig. 1e with no any blue dots existence in the film. Then the conventional devices were assembled with the configuration of F-doped SnO₂ (FTO)/compact TiO₂ (c-TiO₂)/SnO₂/Perovskite/Spiro-OMeTAD/Au. The optimal doping concentration of compound **1** for device performance was optimized as shown in Fig. 2a. Fig. 2b shows the photocurrent density versus photovoltage (J - V) curves of the optimal device with and without doping. The optimal device with doping compound **1** under reverse-scan direction exhibited a short-circuit current density (J_{SC}) of 23.39 mA/cm², an open-circuit voltage (V_{OC}) of 1.12 V, a fill factor (FF) of 0.80, and the high PCE of 21.41%. This optimal device showed ignorable hysteresis with a J_{SC} of 24.19 mA/cm², a V_{OC} of 1.10V, a FF of 0.80, and the PCE of 21.34% under forward-scan direction. However, the device without doping showed the PCEs of 20.22% and 18.22% under reverse-scan and forward-scan direction, respectively. The hysteresis index (HI = (PCE_{reverse} - PCE_{forward})/ PCE_{reverse}) of the optimal devices with and without doping were calculated to be 0.3% and 9.9%, respectively. Therefore, the doping of the compound **1** reduces largely the hysteresis of the device, which may originate from the reductive defect density in doped perovskite, reduced charge recombination and efficient charge extraction.^[9] The steady-state photocurrent output was conducted under maximum power point (MPP) bias to confirm the reliability of the devices. As shown in Figure 2c, the device with doping exhibits stable photocurrent after 100s continuous illumination compared to continuous photocurrent decrease of control device, indicating that the doping of compound **1** can improve both PCE and light stability. The integration of the external quantum efficiency (EQE) spectra of the devices with and without doping are shown in Figure 2d. The device with doping achieves an integrated J_{SC} of 22.28 mA/cm² while that of control device shows 22.11 mA/cm², which are consistent with the measured values. Figure 2 e-h show the performance parameters of devices with and without doping, indicating the distinct improvement of devices with doping compound **1**.

To confirm the interaction between the compound **1** and perovskite, we performed X-ray photoelectron spectroscopy (XPS) analysis of the perovskite films. The limidazo[5,1,2-*cd*]indolizine core has strong π system, which is expected to form π -Pb²⁺ with the under-coordinated Pb²⁺ to reduced defects density of the perovskite.^[10] As shown in Figure 3a, our hypothesis was

COMMUNICATION

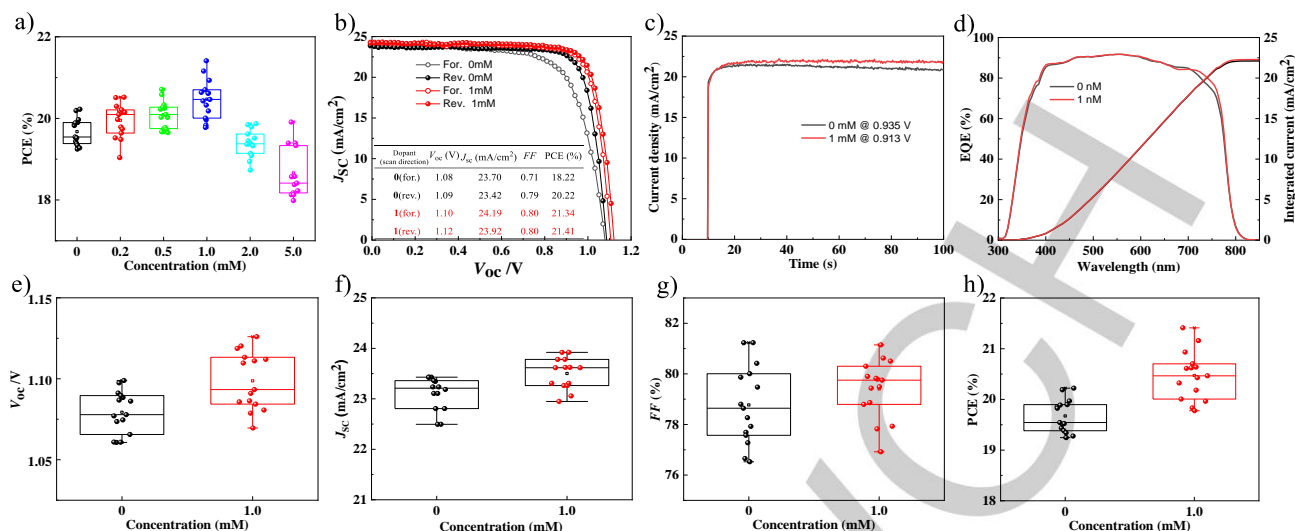


Figure 2. (a) PCEs of devices based on various concentration (mmol/ml) of the compound **1**. (b) J - V curves for the best-performing devices based on the perovskite films with and without doping under illumination of AM 1.5G 100 mW/cm². The inset is the corresponding performance parameters. (c) Maximal steady-state photocurrent output of the champion devices based on the perovskite films with and without doping at the maximum power point. (d) EQE curves of PSCs based on the perovskite films with and without doping. The reverse scanning performance parameters (e) V_{oc} , (f) J_{sc} , (g) FF , (h) PCE of 15 devices based on the perovskite films with and without doping.

verified by the peaks shift (from 141.85 to 141.30 eV for Pb 4f_{5/2} orbit while from 137.05 to 136.4 eV for Pb 4f_{7/2} orbit), indicating the higher electron density environment around Pb²⁺ cation created by the compound **1**. The quality of the perovskite films on glass was further evaluated by the steady-state photoluminescence (PL) and time-resolved photoluminescence (TRPL) decay measurements. In Figure 3b, the PL intensity of the perovskite film with doping compound **1** is significantly enhanced compared to that of the control film, indicating the high radiative recombination of the perovskite film with doping, which also suggests that the nonradiative recombination is restrained in doped perovskite film. Additionally, the PL peak of the doped film shows a blueshift of 2 nm compared with that of the control film, indicating that there is a decrease of defects density resulting possibly from the passivation interaction between the π electrons of the compound **1** and the Pb²⁺ in perovskite.^[11] Figure 3c shows the TRPL decay curves. The fitted parameters are summarized in Table S4. The average PL lifetimes (τ_{ave}) were calculated from the following equation (1):^[12]

$$\tau_{ave} = \frac{\sum A_i \tau_i^2}{\sum A_i \tau_i} \quad (1)$$

We obtained the τ_{ave} values are 67 ns and 44 ns for perovskite films with and without doping, respectively. As our expected, the τ_{ave} is enhanced after doping, showing that the compound **1** reduces the nonradiative recombination of the perovskite film. In order to quantitatively estimate the defects density in perovskite, the space charge limited current (SCLC) method with the device structure of FTO/c-TiO₂/mp-TiO₂/Perovskite/PCBM/Au was exploited. The J - V curves were obtained in the dark. As shown in

Figure 3d, the trap-filled voltage (V_{TFL}) can be obtained through a kink point between the ohmic and the trap-filled regimes.^[13] The defects density (N) is calculated from the Equation (2) below:

$$V_{TFL} = \frac{eNL^2}{2\epsilon\epsilon_0} \quad (2)$$

Where e is the elementary charge, L is the thickness of perovskite film, ϵ is the relative dielectric constant of the perovskite and ϵ_0 is the vacuum permittivity. As shown in Figure 3d, the defect density was calculated to be 1.66×10^{16} and 3.39×10^{16} cm⁻³ for perovskite films with and without doping, which points out that the doping of compound **1** can effectively reduce the electron defects density of the perovskite film. Besides, the recombination dynamic in PSCs is frequently investigated through the dependency of V_{oc} on light intensity according to the following equation (3),

$$V_{oc} = nkT/q \ln(I) \quad (3)$$

where n , k , T , and q are ideal factor, Boltzmann constant, absolute temperature and the electron charge.^[14] When the ideal factor is close to 1, the effect of Shockley-Read-Hall recombination can be neglected. From the slope of the curves in Figure 3e, the fitting result decreased from 1.67 to 1.40 for doping device, suggesting that the doping of compound **1** can reduce the defects density and suppress charge recombination, in well consistent with the XPS, PL, TRPL and SCLC measurement results. Besides, the transient photovoltage (TPV) decay of perovskite films with and without doping PDPII were also measured. As shown in Figure S3 that the film with doping shows longer charge recombination constant, indicating better carrier extraction of the doped film.

A better insight into the interactions between the compound **1**

COMMUNICATION

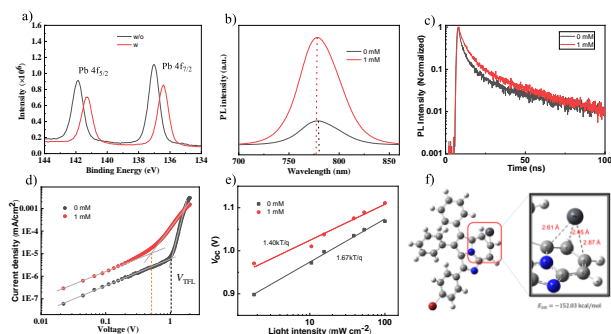


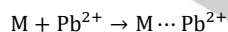
Figure 3. (a) Pb 4f XPS spectra of the control and the doped films. (b) PL spectra and (c) time-resolved PL decays of the perovskite films with and without doping. (d) The dark J–V curves of devices based on the perovskite films with and without doping. (e) V_{oc} of devices as function of illumination intensity. (f) The ideal model of interaction between the compound **1** and Pb^{2+} cation in perovskite.

and perovskite was illustrated by density functional theory (DFT) calculations, where the perovskite was assumed to be PbI_2 -terminated system (there are detailed calculation parameters in the Supporting Information). The optimized model of the compound **1** and perovskite (Pb^{2+}) is shown in Fig. 3f with shortest length of 2.45 Å. Partial electron density of C=C bond donated to Pb^{2+} cation causes slight distortion of π -plane and the decrease of the bond order. In computational chemistry, the interaction energy between A and B is determined by E_{int} , which is estimated by the following equation (4):^[15]

$$E_{int} = E_{AB} - (E_A + E_B) + BSSE \text{ (basis set superposition error)}$$

$$= E_{AB}^{corr} - (E_A + E_B) \quad (4)$$

where E_{AB} is the energy of complex AB, $E_A + E_B$ is the sum energy of monomers, and E_{AB}^{corr} is the counterpoise corrected energy of the complex. The corrected complexation energy was simulated to be -152.03 kcal/mol. We also analyzed the predicted thermochemistry data of the above ideal model in gas phase at 298.15 K under 1 atm. Assuming the reaction is



Where M represents the doping molecule. Since in any certain temperature, there are

$$\Delta_r H_m = \sum_{\text{products}} (\varepsilon_0 + H_{corr}) - \sum_{\text{reactants}} (\varepsilon_0 + H_{corr})$$

$$\Delta_r G_m = \sum_{\text{products}} (\varepsilon_0 + G_{corr}) - \sum_{\text{reactants}} (\varepsilon_0 + G_{corr})$$

$$\text{and } \Delta_r G_m = \Delta_r H_m - T \Delta_r S_m$$

where $\Delta_r H_m$, $\Delta_r S_m$ and $\Delta_r G_m$ are the change of enthalpy, entropy and Gibbs free energy per mol reaction.^[16] $\varepsilon_0 + H_{corr}$ and $\varepsilon_0 + G_{corr}$ are the sum of electronic and thermal enthalpy, the sum of electronic and thermal free energy, respectively. It can be easily figured out that the reaction was favored by both enthalpy with

$\Delta_r H_m = -488.66 \text{ kcal mol}^{-1}$ (1 Hartree = 627.509469 kcal mol⁻¹) and Gibbs free energy with $\Delta_r G_m = -481.02 \text{ kcal mol}^{-1}$. Although accompanying with the decrease of entropy ($\Delta_r S_m = -25.63 \text{ cal mol}^{-1} K^{-1}$), the strong exothermal effects suggested a thermodynamically spontaneous process at room temperature in gas phase.

To further gain insight into the mechanism responsible for the improvement of device performance, kelvin probe force microscopy (KPFM) was utilized to study the surface potential change of perovskite films. Figure 4a, b are the topography images of the perovskite films without and with doping. The corresponding contact potential difference (CPD) images are shown in Figure 4c, d, respectively. A deeper surface potential was clearly observed for the perovskite film with doping, as reflected from CPD values ($-200 \pm 16 \text{ mV}$ for doping film and $-95 \pm 18 \text{ mV}$ for control film) in Figure 4e. The ultraviolet photoelectron spectroscopy (UPS) analysis was then exploited to verify the KPFM results. As shown in Figure S4 and S5, the Fermi levels and valance band edges are obtained as -4.61 eV and -5.64 eV, -4.92 eV and -5.83 eV for perovskite films without and with doping, respectively. The doping of compound **1** leads to a downward shift of Fermi level, which is consistent with the KPFM results. The deeper CBM of doped perovskite film can reduce the recombination possibility of electrons from the perovskite with the holes in HTL, which is beneficial to the enhancement of V_{oc} . Additionally, the Fermi level is closer to valance band edge of the doping film compared to that of the control film (Figure 4f), enhancing hole extraction and benefiting for the higher V_{oc} in doped device.^[17]

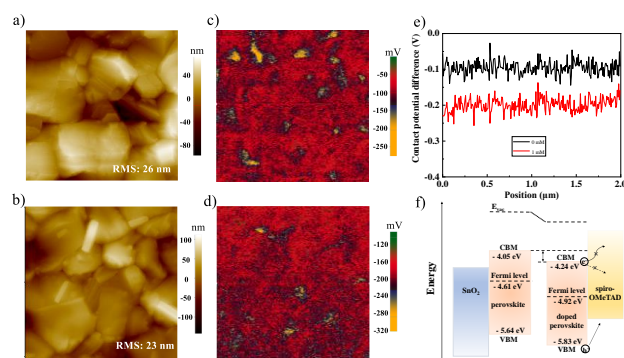


Figure 4. Surface morphology and potential of (a), (b) AFM, and (c), (d) KPFM images of pristine and doped perovskite films. (e) Potential profiles along the indicated line. (f) Energy band diagram of the charge transportation layers and perovskite films with and without doping.

To check whether Br in compound **1** offers additional benefit in improving device performance, we synthesized Cl-, I- substituent PDPIIs (see the details in Supporting Information). Both devices with doping Cl-PDPII and I-PDPII showed better PCEs than that of the devices without doping. However, the devices with doping

COMMUNICATION

the compound **1** (Br-PDPII) showed the best results (Figures S6 and Table S5), mainly due to higher V_{oc} and FF values.

Finally, the stability of the device with doping was investigated. As shown in Figure S7, the un-encapsulation device with doping **1** exposed to air with a relative humidity (RH) of around 20% retained ~ 94% of the initial PCE after 1300h of storage, whereas an un-encapsulation device without doping kept ~ 87% of the original value under the same conditions. The light stability of encapsulated devices with and without doping was tested as shown in Figure S8. The doped device remained basically unchanged after 270 h continuous irradiation at MPP condition. However, the control device decayed to 60% of its original PCE after 240 h. We also conducted high humidity (RH 80%) and high temperature (150°C) measurement of perovskite films without and with doping. We took pictures of the films both from front and back sides. As shown in Figure S9, the control film began to decay at 0.5h under RH 80%. However, the doped film shows sign of degradation at around 2h. Figure S10 shows the thermal stability of perovskite films under 150 °C and RH 25% in air. We can see that the doped film remains unchanged after 8h compared to the control film decomposition at 6h. All above data shows that the introduction of PDPII could enhance the stability of perovskite films and PSCs.

In summary, a chemical doping approach was utilized to improve the performance of PSCs, using an organic small molecule PDPII based on the imidazo[5,1,2-cd]indolizine core, on one side passivates defects, on the other side downshifts valence band maximum to improve hole extraction. As a result, the device with negligible hysteresis (HI of 0.3%) were achieved compared to the control device (HI of 9.9%). Taking advantage of multiple techniques to characterize the reduction of defects density and efficient depression of charge recombination are detailed illustrated in this paper, where also shows that organic chemistry could provide efficient tools to improve the performance of PSCs.

Acknowledgements

The work was supported by the Taishan Scholars Project of Shandong Province. We are grateful to Dr. Chongwen Li and Dr. Xiao Liu for their beneficial discussion.

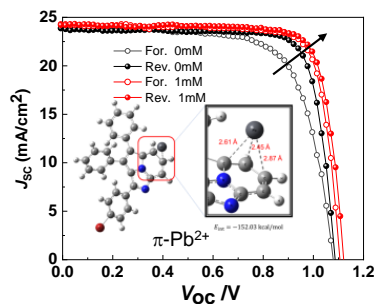
Keywords: Perovskite solar cells • π -Pb²⁺ interaction • defects density • charge extraction • organic small molecule

[1] a) K. Galkowski, A. Mitioglu, A. Miyata, P. Plochocka, O. Portugall, G. E. Eperon, J. T.-W. Wang, T. Stergiopoulos, S. D. Stranks, H. J. Snaith, R. J. Nicholas, *Energy Environ. Sci.* **2016**, *9*, 962–970; b) T. Baikie, Y. Fang, J. M. Kadro, M. Schreyer, F. Wei, S. G. Mhaisalkar, M. Grätzel, T. J. White, *J. Mater. Chem. A* **2013**, *1*, 5628–5641; c) Q. Dong, Y. Fang, Y.

Shao, P. Mulligan, J. Qiu, L. Cao, J. Huang, *Science* **2015**, *347*, 967–970.
 [2] a) A. Kojima, K. Teshima, Y. Shirai, T. Miyasaka, *J. Am. Chem. Soc.* **2009**, *131*, 6050–6051; b) <https://www.nrel.gov/pv/cell-efficiency.html>, (accessed: September 2020).
 [3] B. Ehrler, E. Alarcón-Lladó, S. W. Tabernig, T. Veeken, E. C. Garnett, A. Polman, *ACS Energy Lett.* **2020**, *5*, 3029–3033.
 [4] a) S. Xiong, J. Song, J. Yang, J. Xu, M. Zhang, R. Ma, D. Li, X. Liu, F. Liu, C. Duan, M. Fahlman, Q. Bao, *Sol. RRL* **2020**, *4*, 1900529; b) X. Zhu, M. Du, J. Feng, H. Wang, Z. Xu, L. Wang, S. Zuo, C. Wang, Z. Wang, C. Zhang, X. Ren, S. Priya, D. Yang, S. (Frank) Liu, *Angew. Chem. Int. Ed.* **2020**, DOI: 10.1002/anie.202010987; c) S. Chen, Q. Pan, J. Li, C. Zhao, X. Guo, Y. Zhao, T. Jiu, *Sci. China Mater.* **2020**, *63*, 2465–2476; d) L. K. Ono, S. (Frank) Liu, Y. Qi, *Angew. Chem. Int. Ed.* **2020**, *59*, 6676–6698; e) W. Qi, X. Zhou, J. Li, J. Cheng, Y. Li, M. J. Ko, Y. Zhao, X. Zhang, *Sci. Bull.* **2020**, *65*, 2022–2032; f) M. Abdi-Jalebi, M. I. Dar, S. P. Senanayak, A. Sadhanala, Z. Andaji-Garmaroudi, L. M. Pazos-Outón, J. M. Richter, A. J. Pearson, H. Sirringhaus, M. Grätzel, R. H. Friend, *Sci. Adv.* **2019**, *5*, eaav2012; g) E. H. Anaraki, A. Kermanpur, M. T. Mayer, L. Steier, T. Ahmed, S.-H. Turren-Cruz, J. Seo, J. Luo, S. M. Zakeeruddin, W. R. Tress, T. Edvinsson, M. Grätzel, A. Hagfeldt, J.-P. Correa-Baena, *ACS Energy Lett.* **2018**, *3*, 773–778.
 [5] a) W. Chen, Y. Wang, G. Pang, C. W. Koh, A. B. Djurišić, Y. Wu, B. Tu, F.-z. Liu, R. Chen, H. Y. Woo, X. Guo, Z. He, *Adv. Funct. Mater.* **2019**, *29*, 1808855; b) H. Chen, T. Liu, P. Zhou, S. Li, J. Ren, H. He, J. Wang, N. Wang, S. Guo, *Adv. Mater.* **2019**, *32*, 1905661; c) W. Xu, Y. Gao, W. Ming, F. He, J. Li, X.-H. Zhu, F. Kang, J. Li, G. Wei, *Adv. Mater.* **2020**, *32*, 2003965; d) S. Ye, H. Rao, Z. Zhao, L. Zhang, H. Bao, W. Sun, Y. Li, F. Gu, J. Wang, Z. Liu, Z. Bian, C. Huang, *J. Am. Chem. Soc.* **2017**, *139*, 7504–7512; e) W.-Q. Wu, Q. Wang, Y. Fang, Y. Shao, S. Tang, Y. Deng, H. Lu, Y. Liu, T. Li, Z. Yang, A. Gruverman, J. Huang, *Nat. Commun.* **2018**, *9*, 1625; f) Y. Lin, Y. Shao, J. Dai, T. Li, Y. Liu, X. Dai, X. Xiao, Y. Deng, A. Gruverman, X. C. Zeng, J. Huang, *Nat. Commun.* **2021**, *12*, DOI: 10.1038/s41467-020-20110-6.
 [6] a) C.-H. Chiang, C.-G. Wu, *Nat. Photon.* **2016**, *10*, 196–200; b) K. Wang, C. Liu, P. Du, J. Zheng, X. Gong, *Energy Environ. Sci.* **2015**, *8*, 1245–1255; c) Y. Wu, X. Yang, W. Chen, Y. Yue, M. Cai, F. Xie, E. Bi, A. Islam, L. Han, *Nat. Energy* **2016**, *1*, 16148.
 [7] X. Li, C.-C. Chen, M. Cai, X. Hua, F. Xie, X. Liu, J. Hua, Y.-T. Long, H. Tian, L. Han, *Adv. Energy Mater.* **2018**, *8*, 1800715.
 [8] a) D. Bi, C. Yi, J. Luo, J.-D. Décoppet, F. Zhang, S. M. Zakeeruddin, X. Li, A. Hagfeldt, M. Grätzel, *Nat. Energy* **2016**, *1*, 16142; b) Q. Hu, E. Rezaee, W. Xu, R. Ramachandran, Q. Chen, H. Xu, T. EL-Asaad, D. V. McGrath, Z.-X. Xu, *Small* **2020**, *17*, 2005216.
 [9] Y. Wang, X. Liu, Z. Zhou, P. Ru, H. Chen, X. Yang, L. Han, *Adv. Mater.* **2019**, *31*, 1803231.
 [10] T. Niu, J. Lu, R. Munir, J. Li, D. Barrit, X. Zhang, H. Hu, Z. Yang, A. Amassian, K. Zhao, S. Liu, *Adv. Mater.* **2018**, *30*, 1706576.
 [11] Y. Shao, Z. Xiao, C. Bi, Y. Yuan, J. Huang, *Nat. Commun.* **2014**, *5*, 5784.
 [12] J. Chen, X. Zhao, S. G. Kim, N. G. Park, *Adv. Mater.* **2019**, *31*, 1902902.
 [13] a) Z. Zhou, Z. Qiang, T. Sakamaki, I. Takei, R. Shang, E. Nakamura, *ACS Appl. Mater. Interfaces* **2019**, *11*, 25, 22603–22611; b) L. Wang, H. Zhou, J. Hu, B. Huang, M. Sun, B. Dong, G. Zheng, Y. Huang, Y. Chen, L. Li, Z. Xu, N. Li, Z. Liu, Q. Chen, L.-D. Sun, C.-H. Yan, *Science* **2019**, *363*, 265–270.
 [14] a) Q. Jiang, Y. Zhao, X. Zhang, X. Yang, Y. Chen, Z. Chu, Q. Ye, X. Li, Z. Yin, J. You, *Nat. Photon.* **2019**, *13*, 500; b) X. Liu, H. Q. Wang, Y. Li, Z. Gui, S. Ming, K. Usman, W. Zhang, J. Fang, *Adv. Sci.* **2017**, *4*, 1700053.
 [15] F. B. van Duijneveldt, J. G. C. M. v. D.-v. Rijdt, J. H. v. Lenthe, *Chem. Rev.* **1994**, *94*, 1873–1885.
 [16] <https://gaussian.com/wp-content/uploads/dl/thermo.pdf>.
 [17] a) H. Kanda, N. Shibayama, A. J. Huckaba, Y. Lee, S. Paek, N. Klipfel, C. Roldán-Carmona, V. I. E. Quélou, G. Grancini, Y. Zhang, M. Abuhelaiga, K. T. Cho, M. Li, M. D. Mensi, S. Kingee, M. K. Nazeeruddin, *Energy Environ. Sci.* **2020**, *13*, 1222–1230. b) F. Ansari, E. Shirzadi, M. Salavati-Niasari, T. LaGrange, K. Nonomura, J.-H. Yum, K. Sivula, S. M. Zakeeruddin, M. K. Nazeeruddin, M. Grätzel, P. J. Dyson, A. Hagfeldt, *J. Am. Chem. Soc.* **2020**, *142*, 26, 11428–11433.

COMMUNICATION

Table of Contents



Featuring a fused tricyclic core, an organic small molecule was intentionally synthesized to reduce defects density and improve hole transportation in perovskite devices via $\pi\text{-Pb}^{2+}$ interaction, confirmed by multiple characterizations and simulation.